Matematisk-fysiske Meddelelser
udgivet af
Det Kongelige Danske Videnskabernes Selskab
Bind **31,** nr. 10

Mat. Fys. Medd. Dan. Vid. Selsk. **31,** no. 10 (1959)

SCATTERING OF 20 MeV α-PARTICLES

BY

H. W. FULBRIGHT, N. O. LASSEN,
AND N. O. ROY POULSEN

København 1959
i kommission hos Ejnar Munksgaard

CONTENTS

Synopsis

Focusing and analyzing magnets for bringing the external cyclotron beam to a shielded room were constructed. An ionization chamber for detecting scattered α's was constructed and the set-up was found to give a resolution of about 1 % in energy.

The energy spectra of scattered α's were measured at 45°, 90°, and 135° for a number of elements. Peaks due to direct interaction processes were observed in all elements except the heaviest, where the α-particles cannot penetrate the barrier. Energy distributions corresponding to α-particles evaporated from the compound nucleus were observed for Ni, Cu, and Zn. From the shape of the spectra the level density for these elements was found, for excitation energies E^* in the region 4—11 MeV, to be proportional to exp (E^*/T) with T = const. rather than to exp $\sqrt{aE^*}$. This does not agree with the simple Fermi gas theory, but is consistent with recent theories taking into account the fact that the nucleons at low excitation energies cannot be regarded as free Fermi gas particles.

The cross section for evaporated α-particles was found to be almost the same at the three angles in high contrast to the single peaks due to direct interactions. Using the experimentally determined level density functions, the cross sections for (α, α') compound nucleus scattering were calculated by means of the statistical theory. The calculated cross sections agree with the measured values within a factor of two.

Printed in Denmark
Bianco Lunos Bogtrykkeri A-S

1. Introduction

An abundance of information accumulated in the past ten years has clearly shown that the well-known theory of nuclear reactions based upon compound nucleus formation is quite inadequate to account for many of the phenomena observed, and a number of theories have been developed to account for special cases of so-called direct interactions, especially BUTLER's theory[1] of the stripping reaction and its extension to include various other types of stripping and pickup reactions. In many cases, these theories have had outstanding success, and no one can seriously doubt the validity of the mechanisms postulated in those cases. As matters now stand, additional explorations of direct interaction processes are vigorously under way in many laboratories. The results to be described below give evidence of the importance of both the compound nucleus mode and a direct interaction mode of inelastic scattering of α-particles from nuclei.

The original motivation for our efforts came from the work of COHEN[2] on the inelastic scattering of 23 MeV protons from medium Z and high Z nuclei, experiments which showed, among other things, a systematic enhancement of the intensity of scattered protons leaving the target nucleus with an excitation of 2 to 3 MeV. We started out to see whether similar results would be obtained in a study of the inelastic scattering of 20 MeV α-particles. Of course, the higher Coulomb barrier in our case would prevent us from obtaining comparable data above the medium region, but we hoped to shed some light upon the mystery posed by the proton work. As it turned out, our work, which covered relatively few nuclei in the medium Z range, yielded results similar to Cohen's in showing strong α-particle groups apparently corresponding to individual low-lying excited states, and in showing the onset of a continuum smoothly rising with increasing energy of excitation of the residual nucleus, but it cannot be said to reproduce the regularities in the intensity patterns found for various nuclei in the proton case.

2. Experimental Arrangement

The overall arrangement of the experimental apparatus is shown in Fig. 1. The 20 MeV deflected, analyzed, and focused α-particle beam of the Copenhagen cyclotron was used. The particle detector was an ionization chamber featuring fast electron collection and a Frisch grid. The scattering chamber had ports for supporting the ionization chamber at an angle of observation of 45°, 90°, or 135°. The beam was collected in a Faraday cup connected to an accurate and stable electronic integrator circuit.

Beam Handling System

Before the experiments could be undertaken it was necessary to obtain a deflected beam and to prepare a magnet system for handling it. This work required several months.

When the Copenhagen cyclotron was rebuilt, an internal deflector was installed inside one of the dees, but, up to the time when our plans began to develop, it had never been put into service. After some weeks of careful adjusting of the position controls of the deflector system, a fairly satisfactory set of operating conditions was found and a beam of 5 to 10 microamperes of α-particles was obtained at the opening in the stem of the second dee through which the deflected beam passed after leaving the dee containing the deflector plates. There was some trouble with deflector sparking, especially at the beginning of operation when a conditioning period of five to ten minutes was required before the full 40 to 50 KV potential difference could be applied.

The beam emerged from the dee chamber through a special valve and lock system just before the horizontal center line on Fig. 1. Ray-tracing experiments showed that it was diverging horizontally as if the rays came from a fairly well defined virtual source about 70 cm behind the exit port. To reduce the spreading of the beam a special lens was installed.

Gradient lens 1 has a focusing action on the horizontal motion of the particles. Its pole tips have flat surfaces tilted together at large radii. Flux for its field comes from the poles of the cyclotron through two stacks of iron flux bars trimmed empirically to terminate at such spots on the outer surfaces of the pole pieces of the gradient lens that the desired approximately constant gradient field distribution was obtained in the gap. Ray-tracing experiments showed that most of the particles emerging from gradient lens

1 were moving almost exactly parallel to each other horizontally, while diverging slightly vertically.

To cause the beam to converge horizontally, as well as to bend the beam into a more favourable direction for later use, gradient lens 2 was added.

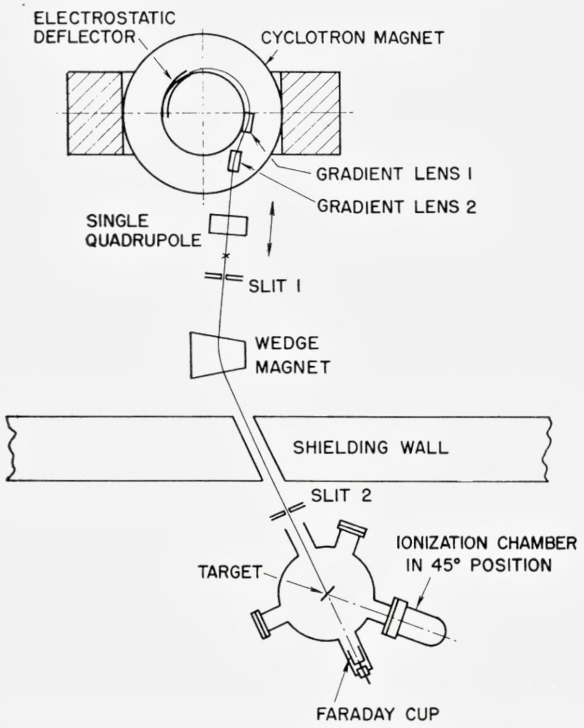

Fig. 1. Overall experimental arrangement, not drawn to scale.

This is a complete magnet situated between the coil tanks of the cyclotron magnet. Its field is in the reverse direction. Experience showed that the magnet could not function if placed within about 30 cm of the cyclotron magnet poles, apparently because of saturation effects. The position finally chosen is the closest one feasible. The current for the coils of gradient lens 2 comes directly from the cyclotron generator; in fact, the coils (of copper strips, 3×30 mm^2) are connected directly in series with the cyclotron magnet coils.

So far as the horizontal motion was concerned, gradient lenses 1 and 2 had the effect of producing a focus at the position indicated by the small

x in Fig. 1. The fluorescent spot actually observed there on a quartz plate had a width of the order of 3 mm with a total vertical extent of about 5 cm. A vertical line of some sort was, of course, to be expected as a consequence of the slight initial vertical divergence of the beam and the inevitable vertical defocusing in gradient lenses 1 and 2. To complete the condensing of the beam a single quadrupole lens with hyperbolic pole tips was added. This lens has a defocusing action in the horizontal direction and a focusing action in the vertical direction. It was mounted on a cart which could easily be moved back and forth parallel to the direction of the beam; the adjustable position was necessary so that the relative effect of the quadrupole lens in the horizontal and vertical directions could be varied. This, together with a variation in the magnetizing current, permitted us to focus the beam as a spot centered on a predetermined point, the center of slit 1 in Fig. 1. The spot turned out to be somewhat fuzzy. It was about 7 mm wide and 12 mm high as judged by observations on a fluorescent plate.

Shortly after this part of the system was completed, some successful preliminary experiments were made with a scattering chamber placed inside the cyclotron room, just past slit 1, but as soon as possible the beam was brought through the shielding wall into an experimental room where the final measurements were made.

The wedge magnet was designed, according to the method of Cross[3], to have the same focal length in the vertical and horizontal directions and to focus an image of slit 1 at the position of slit 2. Of course, what is to be expected at slit 2 is a blurred energy spectrum of the α-particles emerging from slit 1, spread out in the horizontal direction. The particles passing through slit 2 should have a restricted energy spread, which in this case was to be of the order of a few tenths of a percent, the best figure being about 0.2 $^0/_0$ for very narrow slits. No measurement of the actual spread was ever made; the resolution of our ionization chamber spectrometer was insufficient to show the existence of an energy spread.

Because the magnet was designed by a simple method which could not take into proper account fringing field effects, especially those due to the rather extended air-cooled coils, it was mounted on a base which could be moved roughly at right angles to the direction of the beam, and in addition could be rotated. In making the final adjustments on the beam system we used both of these motions, together with variations in the positions of slit 2 (both directions) and the two controls for the quadrupole lens. We were never able to show that the wedge magnet worked as planned, but the quadrupole magnet gave an independent control of the vertical focal posi-

tion, and a satisfactory current of the order of 0.1 microampere was obtained.

Unfortunately this much current could not always be obtained. A loss of current was sometimes accompanied by a lateral motion of the condensed beam across slit 1. A variable resistor shunted across the coils of gradient lens 2 helped to minimize the trouble, but was not sufficient. The most likely explanation for the variation in intensity is that very small variations in the positions and shapes of the iron vacuum chamber lids of the cyclotron from one period of use to another produced changes in the magnetic field of the cyclotron which, in turn, caused (a) a change in the radial oscillations of the particles while they were rotating, and (b) small variations in the trajectories of the particles after deflection. Similar effects have been observed elsewhere. This effect could presumably be reduced greatly by securing better the "fixed" spacing of the lids with respect to the magnet pole tips*.

The Ionization Chamber

The scattered α-particles were observed by means of a fast, electron collection type ionization chamber having the geometry shown approximately to scale in Fig. 2**. α-particles scattered from the foil in the center of the scattering chamber passed through a 1.2 mg/cm^2 mylar window coated on its inner surface with an electrically grounded semi-transparent evaporated film of aluminum. The window was tilted so that the particles entered at an angle of 23° with respect to the normal to its surface. The tilt was an unnecessary refinement added for reasons independent of this experiment. The collector was a ski-shaped strip of brass about 1 cm wide, supported by its connecting electrode. The grid was a 0.2 mm wire wound back and forth in 0.3 mm slots milled in a brass frame with a center-to-center spacing of 3 mm. The size of the opening in the frame was 4.0 cm × 12.5 cm. The grid structure was supported by its connecting electrode. The insulators were made of Teflon (CF_4). Another insulator (not shown) prevented accidental rotation of either the collector or the grid.

* W. P. Alford has shown that similar symptoms observed in the behaviour of the variable energy cyclotron at the University of Rochester were associated with changes in the lid positions and with quite strong variations in the amplitude of radial oscillations. Secure wedging of the lids cured the trouble.

** For a description of the operating principles of this kind of chamber, see Rossi and Staub, "Ionization Chambers" The McGraw-Hill, New York (1949) or Handbuch der Physik, XLV, Ch. 1; J. Springer, Berlin (1958).

The window was held in a special removable frame. The window-to-frame and frame-to-chamber seals were made with O ring gaskets, as were all the other removable seals. The window was supported by a polished brass surface containing 73 1 mm diameter holes drilled parallel to the

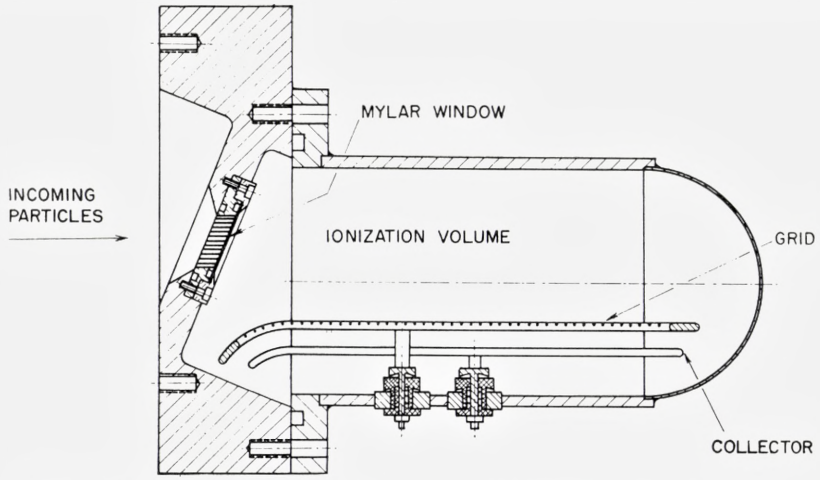

Fig. 2. Gridded ionization chamber used as the charged particle detector.

direction of the scattered beam in a regular pattern, all lying within a 1.5 cm diameter circle.

A hot calcium purifier (not shown) was connected by means of $^1/_4$ inch copper tubing to the top and bottom of the cylindrical section of the chamber wall so that the filling gas could circulate by thermal convection. The purifier was very effective in cleaning the gas, especially just after the chamber had been worked on, then reassembled. Even though meticulous care was taken in cleaning all chamber parts with organic solvents and with a water solution of detergent, the behaviour of the ionization chamber suggested that electronegative gases given off by the walls were steadily removed by the action of the purifier during the first day or so of its operation.

Various gases and mixtures were employed. The mixture most commonly used was argon plus 5 to 20 % of CH_4. The pressure was ordinarily about 3 atmospheres. The grid was maintained at about +1500 volts, the collector at about +3000 volts. Under these conditions, good saturation curves were obtained after purification, there was no noticeable loss of electrons to the grid wires, and the pulse height resolution was excellent.

The preamplifier of an EKCO Type N568 amplifier was attached directly to the ionization chamber by means of a shield. The input wiring of the preamplifier was modified slightly to reduce capacitance. The amplifier proved exceptionally fine for our purposes. Its output was connected to a 99 channel Philips Balham pulse height analyzer.

The stability of the system against both long- and short-time drift of calibration was excellent. Careful measurements made with the help of a pulser based on a vibrating mercury relay showed an accurately linear input pulse height *vs* output pulse height relationship. All our experience with α-particles indicated that a linear relationship also exists between the energy lost by α-particles in the $A + CH_4$ mixture and the number of electrons collected, but this relationship was not the subject of an especially careful investigation.

The resolving power of the system was investigated by means of 5 MeV protons from the cyclotron scattered from a thin Al foil. Peaks from elastic scattering and inelastic scattering with the excitation of the states at 0.84 and 1.01 MeV were sharply resolved, with widths of about 80 keV (full width at half-maximum). With 8.8 MeV α's from a ThC' source or 20 MeV α's from the cyclotron the width was about 130—200 keV.

In most experiments, a continuous low-lying spectrum of pulses due to fast protons entering the chamber through the window, or generated in the chamber by neutrons passing through it (in many cases recoil protons from the CH_4 gas), was observed. The highest pulses of this sort were due to protons having just enough energy to traverse the length of the active volume of gas before coming to rest. Ordinarily, the corresponding energy limit was about 5 MeV.

3. Experimental Results

Carbon and Oxygen

The scattering from these substances has not been studied in detail, but, since both of them appear very frequently as impurities in targets, it was felt to be of some importance to know the rough appearance of the spectra. As an example, the spectrum obtained at 45° with a mylar target ($C_{10}(H_2O)_4$) is shown in Fig. 3. The peak indicated by an arrow on the right side of Fig. 3 was taken to be that due to elastic scattering from O^{16}. The expected positions for peaks corresponding to various known states

of O^{16}, C^{12}, and C^{13} were then calculated. Some are indicated by arrows in Fig. 3. The peak at 6.1 MeV excitation may be due to either or both of the known levels in O^{16} at 6.05 and 6.13 MeV; the next peak similarly may be due to either or both of the levels at 6.9 and 7.1 MeV; and one we

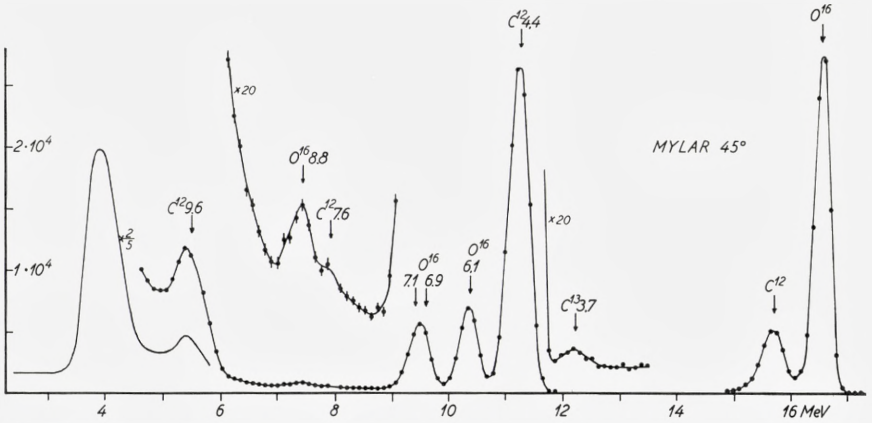

Fig. 3. Spectrum of α-particles scattered from a mylar foil 2.3 mg/cm². Scattering angle 45°. The abscissae are the energy dissipated by the scattered particles inside the ionization chamber, without corrections for absorption in the window of the ionization chamber and in the scattering foil.

have attributed to the known level at 8.8 MeV. These assignments are strengthened by the fact that the four peaks disappear almost entirely if polystyrene is substituted for the mylar scattering foil.

In C^{12}, the first three known levels are 4.43, 7.6, and 9.6 MeV. They are all seen, the 4.43 MeV level very strongly, the corresponding peak being about five times higher than the elastic C^{12}-peak. The 9.6 MeV level also appears rather strongly, whereas the 7.6 MeV level is very weak. In fact, in the mylar curve, the latter is not even certainly detectable; however, when polystyrene is used as a target, the neighbouring O^{16}-peak has disappeared and now the C^{12}-level is clearly seen. To the right of the 4.43 MeV peak, a weak peak is seen; it is also seen in the polystyrene curve and we ascribe it to the second excited level in C^{13} (known levels in C^{13} are 3.09, 3.68, and 3.86 MeV in this region).

The position of the high peak at about 4 MeV depends on the pressure in the ionization chamber, which shows that it is caused by particles passing through the chamber. We think it is due to recoil protons from the hydrogen in the mylar target. Such protons would have about 6.3 MeV, but the range

would be longer than the length of the ionization chamber, and hence only part of their energy would be spent in ionizing the gas in the ionization chamber.

Magnesium

Several preliminary short runs were made with a target of magnesium evaporated onto a thin gold foil. The well-known levels at 1.37 and

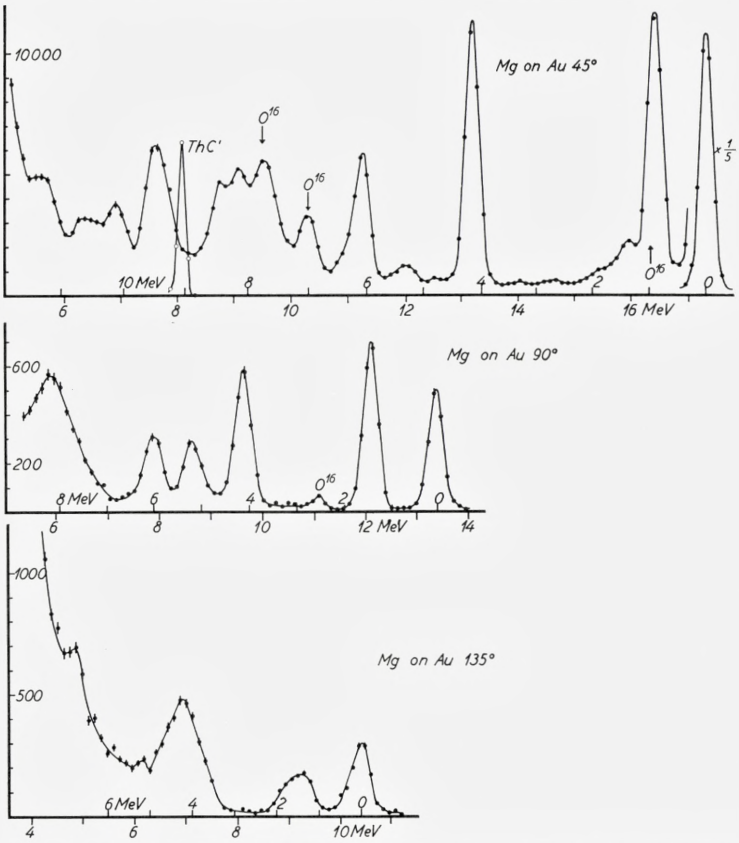

Fig. 4. Spectra of α-particles scattered from a layer of magnesium evaporated onto a 0.16 mg/cm^2 gold foil. The scale below the axis of abscissae gives the energy dissipated inside the ionization chamber. The scale above the axis gives the corresponding excitation energy of the residual nucleus, assuming that Mg^{24} is responsible for the scattering. For Mg^{26}, the scale values are 0.1—0.2 MeV too low. When calculating the scale, absorption in the chamber window and the scattering foil was taken into account. The scattering was assumed to take place in the mid-plane of the magnesium layer. Integrated doses of primary α's 50, 6, and 10 μ Coulomb for 45°, 90°, and 135°, respectively.

4.2 MeV in Mg^{24} are seen at all three angles (Fig. 4), though not with the same intensity ratio. In the 135° direction, these are the only ones visible above the proton background, whereas in the 90° direction three more peaks corresponding to higher excitation energies appear, and at 45° discrete peaks are seen for excitation energies up to more than 10 MeV.

At 45° the oxygen impurity in the target causes trouble. The two peaks corresponding to the 6 and 7 MeV levels in O^{16} are both too high

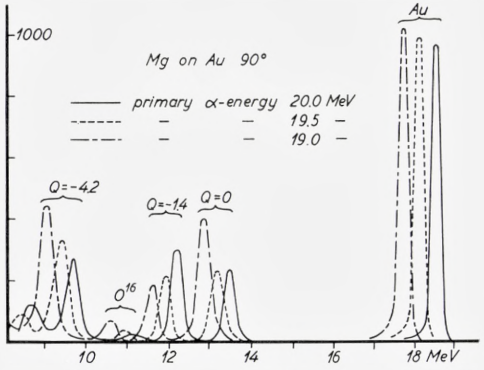

Fig. 5. Spectra of α-particles scattered from magnesium on gold at 90° for different energies of primary α-particles.

as compared with the elastic peak, which shows that at least two peaks corresponding to levels in either of the magnesium isotopes in the region between 6.8—8 MeV have been concealed. The peak with $Q \sim 8.2$ MeV coincides rather closely with the expected position for a known level in Mg^{26} (8.28 MeV) and may perhaps be accounted for in this way. Also the peaks at excitation energies ~ 2.7 and 3.3 MeV may be ascribed to the less abundant isotopes $Mg^{25, 26}$ (see Table 1). The peak at $Q = 6.06$ MeV almost coincides with the expected position for the 4.43 MeV level in C^{12}. However, a control run at 90° together with a comparison with mylar curves at 45° and 90° safely showed that not more than one third (probably much less) of the peak height could be due to carbon.

Though the present curves may be only of little value, a further study has been postponed to a later occasion, because it was felt that, in order to obtain more information, separated isotopes and, especially, more observation angles would be needed. To this decision also contributed the observation that the various peaks are strongly energy dependent. This is illustrated in Fig. 5 which shows the spectra obtained at 90° for slightly

TABLE 1. Magnesium on gold

Known levels in			Q-values of peaks found at		
Mg^{24} 79 %	Mg^{25} 10 %	Mg^{26} 11 %	45°	90°	135°
	0.58 0.98				
1.37			~ 1.4	1.4	1.4
	1.61				
	1.96	1.83	(~ 1.9)		
	2.57 2.74 2.80	2.97	~ 2.7		
	3.40		~ 3.3		
	3.90 3.97	3.97			
4.12 4.25	4.05 4.27 4.42	4.35	4.17	4.17	4.2
4.8	4.67 4.86 4.96	4.86 4.92	~ 4.8		
5.24	5.15 5.34 5.54	5.27 5.32 5.50	5.30	5.20	(5.2)
6.0	6.09 6.25	6.15	6.06	6.0	
6.4	6.54				~ 6.6
6.9 7.4	6.95 7.04	7.29			
		8.28	8.16	8.2	
8.5		8.55	~ 8.5		
		8.93			
9.5			9.5		
		10.08	10.15		

All values in the table in MeV.

different energies of the incoming α-particles. They were degraded in energy by means of aluminum foils placed in the beam before it entered the scattering chamber. The height of the elastic Au-peak varies in the way to be expected from the Rutherford formula. But the heights of the three Mg-peaks vary in different ways.

Aluminum

The spectra obtained at three angles are shown in Fig. 6 and the results are summarized in Table 2. The small peak observed at 45° to the right of the elastic group is probably caused by an iron impurity in the target. As may be seen, the first five levels appear readily in all three directions. The next three levels give only a weaker response. For excitation energies higher than 4 MeV, the level spacing is so small that our energy resolution is insufficient to separate individual peaks and permit their assignment to known levels. For instance, looking at the peak at about 4.5—4.6 MeV, we cannot decide which of the three known levels 4.40, 4.50, and 4.58 MeV is responsible for it or whether more than one of these levels contribute to the spectrum. We cannot even know whether the same levels are responsible for corresponding peaks at different angles. However, peaks are seen up to excitation energies of 10 MeV and more, and since here the level spacing must be quite small, it is obvious that only a small fraction of the highly excited levels show up as single peaks. Therefore the fact that the Q-values corresponding to peaks in the 45°-curve and the 90°-curve are so closely the same seems to indicate that we have to do with the same levels, irrespective of the angle. An exception is the 4.81 MeV level, which is rather strong in the 135° direction, but hardly seen at the other angles. Another exception, the hump in the 135°-curve at about 7.2 MeV excitation energy, may be neglected, since it occurs in a position where the elastic peak from a possible C^{12} impurity would appear.

In Table 2 are given the ratios R_1 between the peak heights at 45° and 90° for some of the peaks. When calculating these values, the different effective thicknesses of the scattering foil at the two angles and the different channel widths were taken into account. The R_1-values show an interesting variation with the excitation energy. The ratios R_2 between peak heights at 90° and 135° are also given.

Nickel

Fig. 7 and Table 3 give the results for nickel. With two exceptions the peaks up to about 4 MeV correspond rather closely to known levels in Ni^{58},

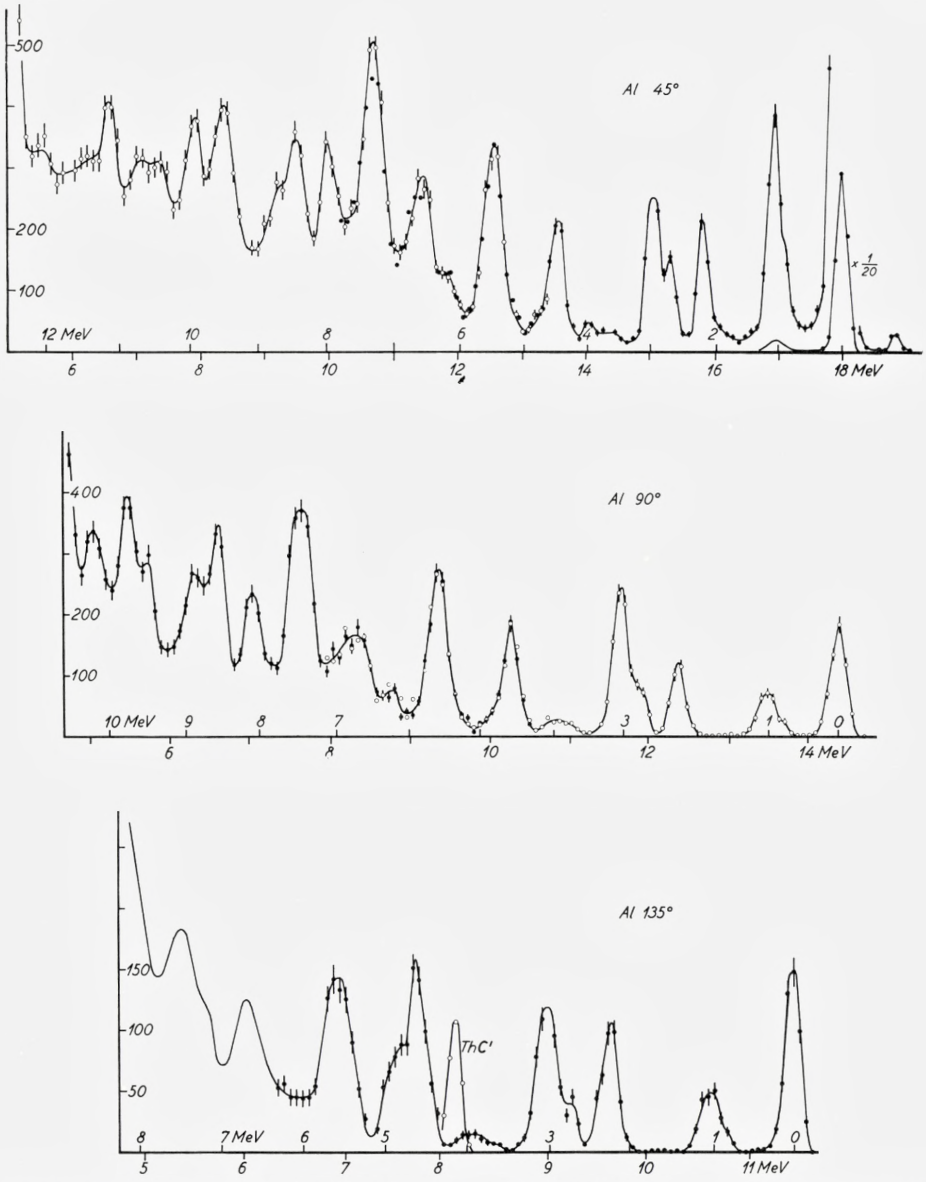

Fig. 6. Spectra of α-particles scattered from an aluminum foil 0.24 mg/cm². Integrated doses of primary α's 40, 40, and 30 μ Coulomb for 45°, 90° , and 135°, respectively. The steep rise in the curves in this figure and the following figures at the left end represents the inset of the proton background. The left part of the 135°-curve in this figure was obtained in a run with less dispersion and covering the whole spectrum.

TABLE 2. Aluminum

Known levels	Q-values of peaks				
	45°	90°	135°	R_1	R_2
	0	0	0	35	0.55
0.84	~ 0.8	~ 0.8	~ 0.8		
1.01	1.06	1.03	1.03	5.8	0.7
2.21	2.20	2.17	2.22	2.0	0.55
2.73	2.7	~ 2.7	~ 2.7	2.3	0.9
3.00	2.95	3.02	3.02	1.2	0.9
3.68	~ 3.7				
3.95 4.05	~ 4.0	~ 4	~ 3.9		
4.40 4.50 4.58	4.5	4.6	4.6	1.1	0.55
4.81	~ 4.8				
5.15 5.24					
5.41 5.42 5.49 / 5.55 5.62	5.5	5.6	5.6	1.3	0.9
5.88					
	~ 6.2	6.2			
	6.6	6.8	6.7	1.8	0.55
			7.2		
	7.3	7.4	7.5	1.5	
	8.0	8.1		1.6	
8.53 8.58 8.69	8.6	8.6		1.1	
8.89 8.94 9.03	~ 8.9	8.8			
9.06 9.17 9.21 / 9.23					
9.38 9.46 9.50 / 9.62 9.66	9.5	9.5		1.6	
	9.9	9.8		1.1	
		10.2			

$$R_1 = \frac{\text{peak height at } 45^\circ}{\text{peak height at } 90^\circ} \qquad R_2 = \frac{\text{peak height at } 90^\circ}{\text{peak height at } 135^\circ}$$

All other values in the table in MeV.

which would be expected, since it is the most abundant isotope (68 %). However, some of the peaks might just as well partly or totally be due to levels in other isotopes. Only in three cases can a safe correlation be established. In the 45-curve a bump is seen for $Q \sim 0.7$ MeV; it has appeared in several runs and we believe it to be real. It is probably due to the known level in Ni^{61}. In the 90°-curve the 1.33 MeV level in Ni^{60} appears. The 1.45 MeV level in Ni^{58} is seen at all three angles.

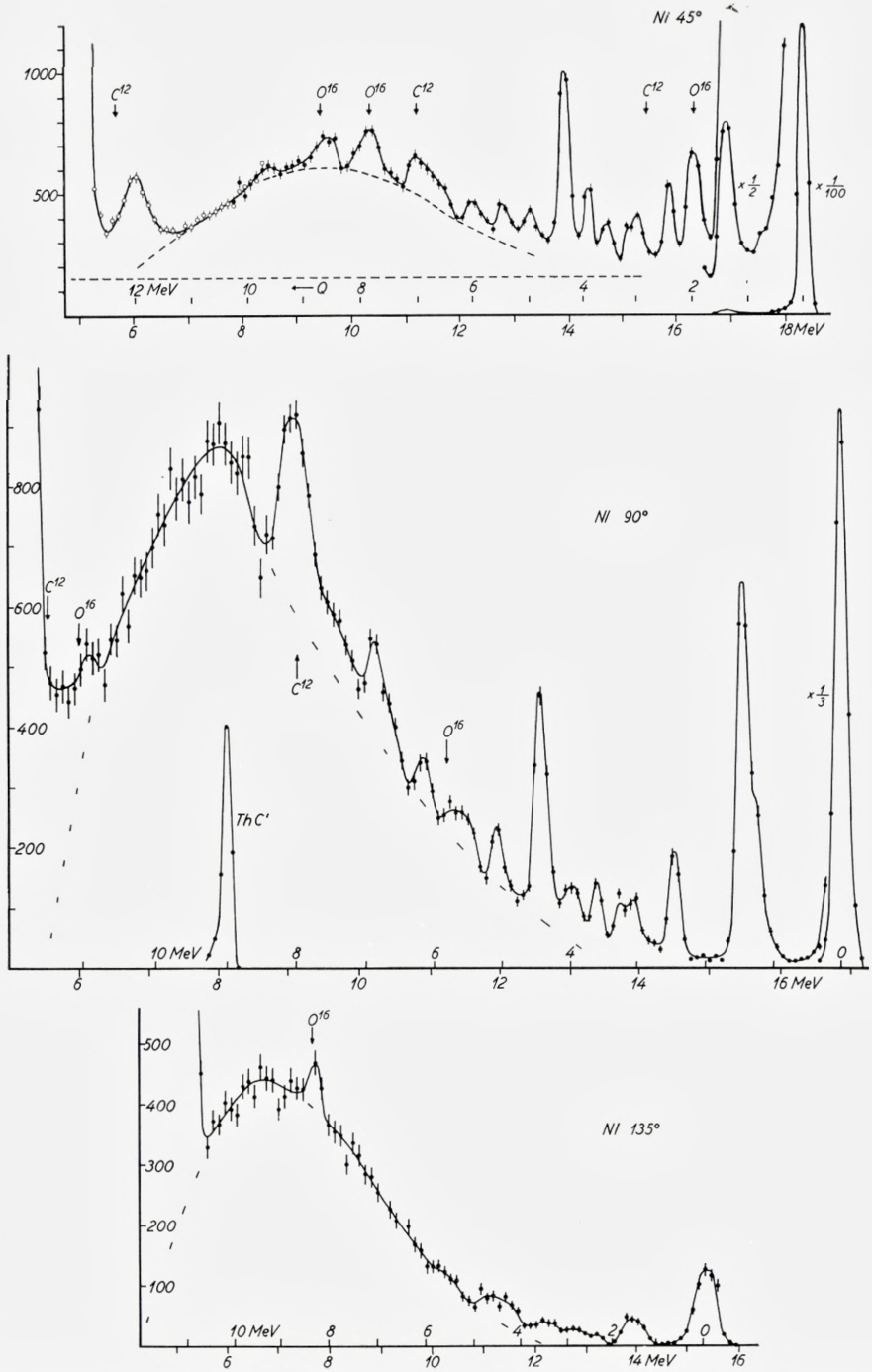

Fig. 7. Spectra of α-particles scattered from a nickel foil. Target thickness 0.5 μ for 45° and 90°, and 1.25 μ for 135°. Integrated doses of primary α's 100, 300, and 40 μ Coulomb for 45°, 90°, and 135°, respectively.

TABLE 3. Nickel

Known levels in			Cohen's peaks	Q-values of peaks		
Ni^{58} 68 %	Ni^{60} 26 %	Ni^{61} 1 %		45°	90°	135°
		0.7		~ 0.7		
	1.33				~ 1.3	
1.45			1.51	1.43	1.45	~ 1.55
	2.16					
	2.28					
2.46	2.50		2.50	2.44	2.44	
	2.62					
2.77						
2.90						
2.94						
3.04	3.12			3.00	3.03	
3.26	3.18		3.20	~ 3.2	3.27	
3.42	3.19					
	3.26					
	3.31					
	3.39					
3.52	3.59			3.6	3.6	
3.59	3.62					
3.63	3.67					
	3.73					
3.77	3.87			3.9	4.0	
3.90	3.89					
4.11	3.92					
	4.00					
	4.04					
	4.08					
				4.35	4.4	
				5.0	5.1	
				5.5	5.7	
				6.0	6.15	
				~ 6.7	6.9	

All values in the table in MeV.

In the 45°-curve, O^{16} gives a high elastic peak and two smaller peaks due to the excited states. The heights of the latter may be estimated from the height of the former, and thus a rough correction indicated by the dotted line can be performed. The arrows show the positions in which the various carbon and oxygen peaks should appear. The 4.43 MeV level in C^{12} is clearly seen; the elastic peak has a height only one fifth of the former and hence cannot be observed. The peak at about 6 MeV is not understood. Since we did not see it when using another Ni target it is probably due to some unknown impurity.

In the 90°-direction the elastic peak from C^{12} is quite strong, whereas O^{16} is hardly seen. In the 135°-direction the oxygen elastic peak clearly appears.

As will be seen later, a strong elastic peak is always accompanied by a tail which for lower energies runs almost horizontal with a height ~ 0.1 % of the elastic peak. The correction is indicated by the dashed line.

The most pronounced feature of the curves, especially in the backward direction and the 90°-direction, is the broad "continuous" distribution of α-particles with energies between 5 and 14 MeV emphasized by the more or less arbitrarily drawn dotted lines. Another striking feature is the absence of high peaks in the backward direction. Though the experimental arrangement may be partly responsible for the difference between forward and backward angles, a thicker target and reflection geometry having been used in the latter case, it is at the first sight evident that the relative intensity of the single peaks as compared to the intensity of the broad continuous distribution is very much smaller at 135° than at the other angles.

In Table 3 and the following tables our peak positions are compared with Cohen's results[5]. He used 23 MeV protons and measured the energy of the scattered protons by means of a magnetic spectrometer with a resolution about twice as good as ours. In Ni the agreement is not particularly good, since we find more levels than he does, some of which are relatively rather strong.

Copper

The results for copper given in Fig. 8 and Table 4 are similar to those for nickel. In an experiment in which an absorber of 11 mg/cm² Al was placed between target and ionization chamber, it was determined that the broad continuous distribution was caused by α-particles. The absorber made the whole spectrum move far to the left, which would not have been

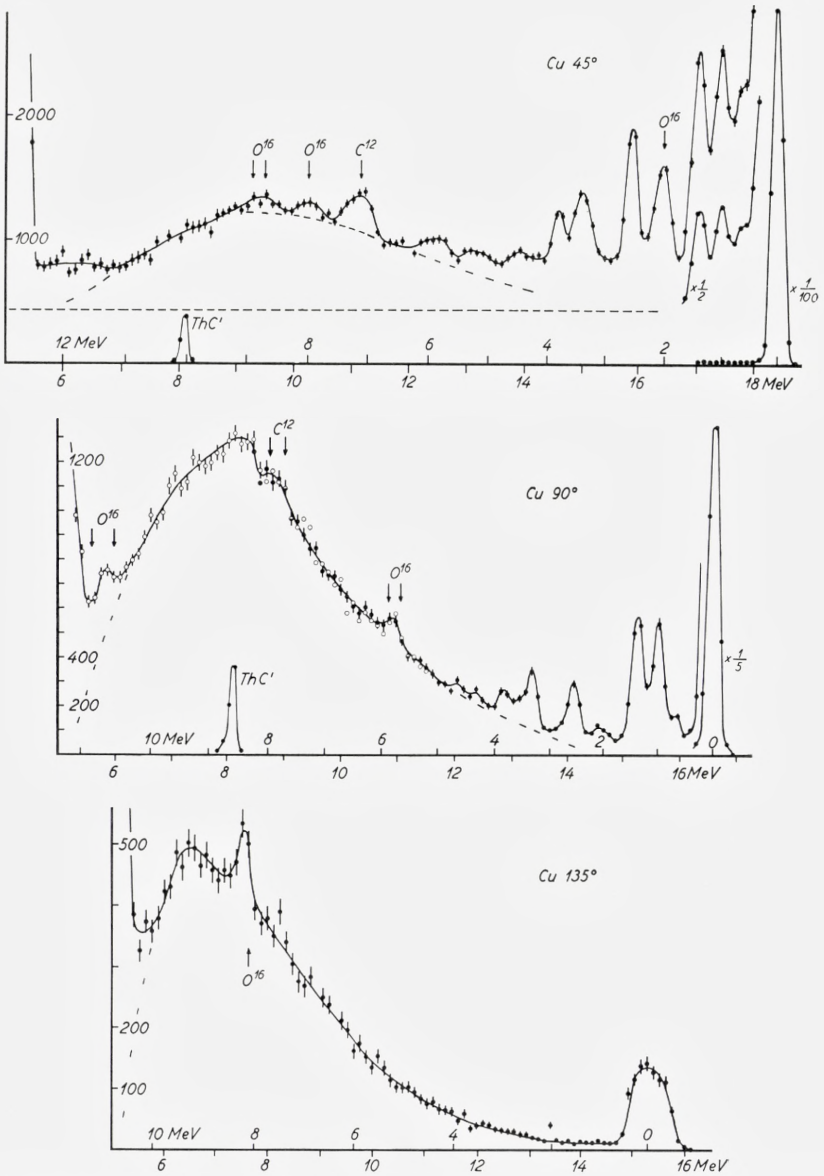

Fig. 8. Spectra of α-particles scattered from a copper foil 2.5 μ. Integrated doses of primary α's 60, 114, and 40 μ Coulomb for 45°, 90°, and 135°, respectively. The two sets of arrows in the 90°-curve give the expected positions for peaks due to oxygen and carbon impurities, assuming that (1) the impurities are located to a surface layer on the side of the foil looking away from the cyclotron or (2) that they are uniformily distributed in the foil.

TABLE 4. Copper

Known levels (4) in		Cohen's peaks	Q-values of peaks		
Cu^{63} 69 %	Cu^{65} 31 %		45°	90°	135°
0.67	0.77	0.70	~ 0.7	~ 0.7	
0.96	1.11	1.01	1.00	0.98	
1.33 1.41		1.38	1.37	1.34	
1.55 1.86	1.48 1.62 1.77				
2.01 2.06 2.08 2.09 2.21	2.09 2.10 2.21	1.97	(0^{16})	2.1	
2.34	2.28 2.35				
2.40 2.49 2.50 2.51 2.53 2.54	2.40 2.53 2.59 2.65	2.51	2.52	2.55	
17 levels	levels < 3.17				
3.21 3.22 3.25 3.29 3.31 3.37 3.40 3.42 3.43 3.46 3.48		3.26	3.4	3.33	
		3.72	3.8	3.85	
			~ 4.4	~ (4.35)	
				~ (4.65)	
			~ 5.2		
			~ 5.9	(0^{16})	

All values in the table in MeV.

the case had it been due to singly charged ions. Note the almost complete absence of any indication for single inelastic peaks at 135°. Note also the good agreement between Cohen's and our peak values in spite of the high number of known levels.

Zinc

Zinc was evaporated in vacuum onto a thin gold foil. The gold backing was only 0.16 mg/cm² but, nevertheless, it gives a considerable background.

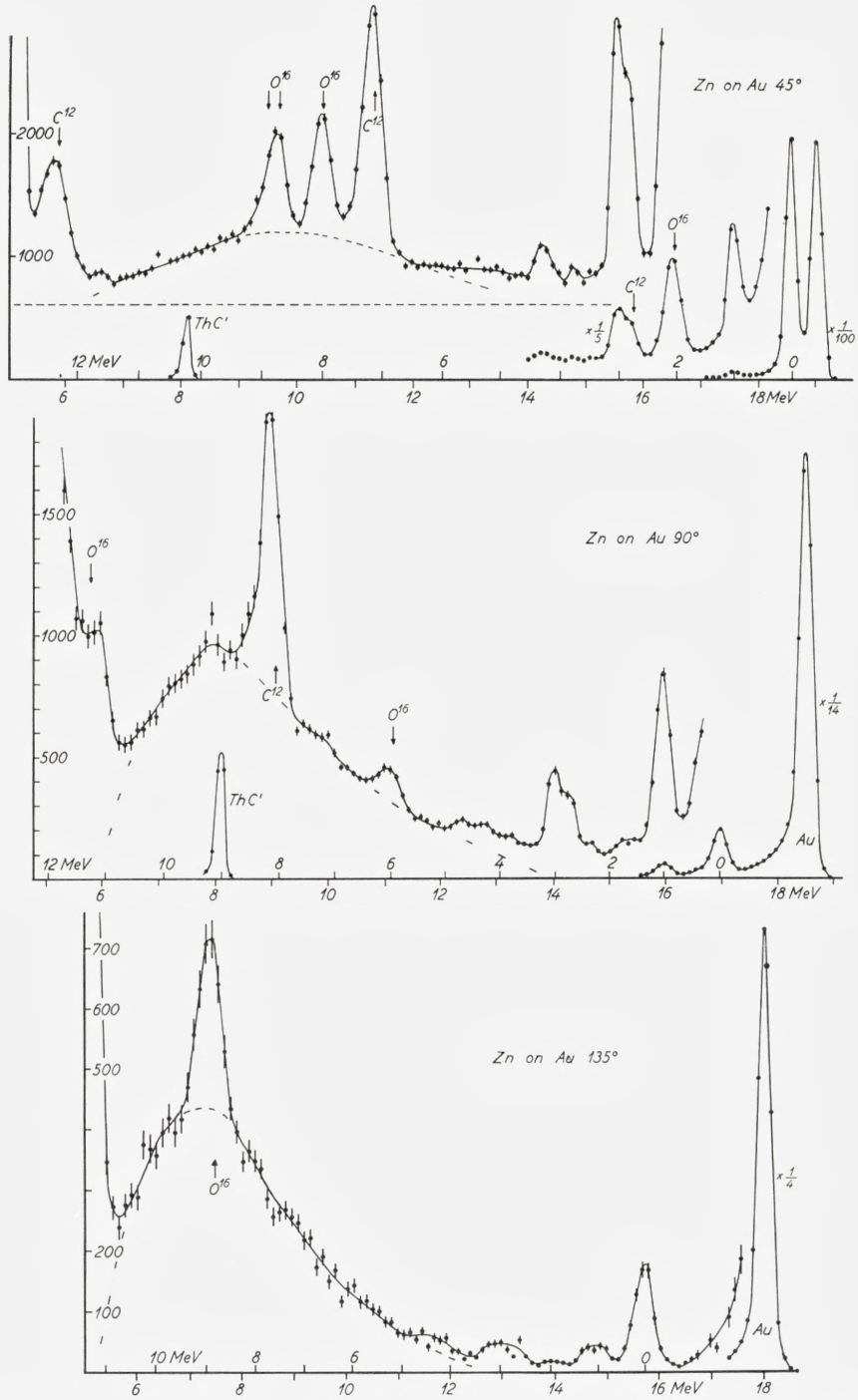

Fig. 9. Spectra of α-particles scattered from a layer of zinc evaporated onto a 0.16 mg/cm² gold foil. Integrated doses of primary α's 75, 160, and 60 μ Coulomb for 45°, 90°, and 135°, respectively.

TABLE 5. Zinc

Known levels in			Cohen's peaks in		Q-values of peaks		
Zn^{64} 49 %	Zn^{66} 28 %	Zn^{68} 19 %	Zn^{64}	Zn^{68}	45°	90°	135°
1	1.04	1.08	1.02	1.07	1.00	1.00	1.1
	1.38						
		1.91	1.83	1.98	(0^{16})	~ 1.7	
2.27			2.13	2.34	(0^{16})	~ 2.3	
				2.68	2.8	~ 2.7	
3.04			3.00		3.0	3.0	~ 3
3.43				3.47			
3.84?				3.8	3.8	(3.8)	
				4.1	4.3	(4.3)	4.5
				4.5			
						(4.7)	
				4.9			
				5.1			
				5.4			

All values in the table in MeV.

The thickness of the Zn-layer was only very roughly known, but from the absolute yield of elastically scattered α-particles it was estimated to be 1.1 mg/cm^2. The appearance of the spectra is dominated by the oxygen and carbon impurities which actually, however, only cause minor difficulties. In the 45°-curve the 4.43 and 9.6 MeV levels in C^{12} are seen, but not the elastic group, because it coincides with a real Zn-peak. Fig. 9 and Table 5 give the results.

Silver

The spectra obtained from silver are shown in Fig. 10. They differ markedly from the earlier spectra. Few strong levels appear. No continuous distribution is seen above background. Table 6 summarizes the results and compares them with Cohen's.

Some levels in Ag are known from Coulomb excitation, among others those at 320, 418, 306, and 412 keV. At 135° and 90° we find a peak, and

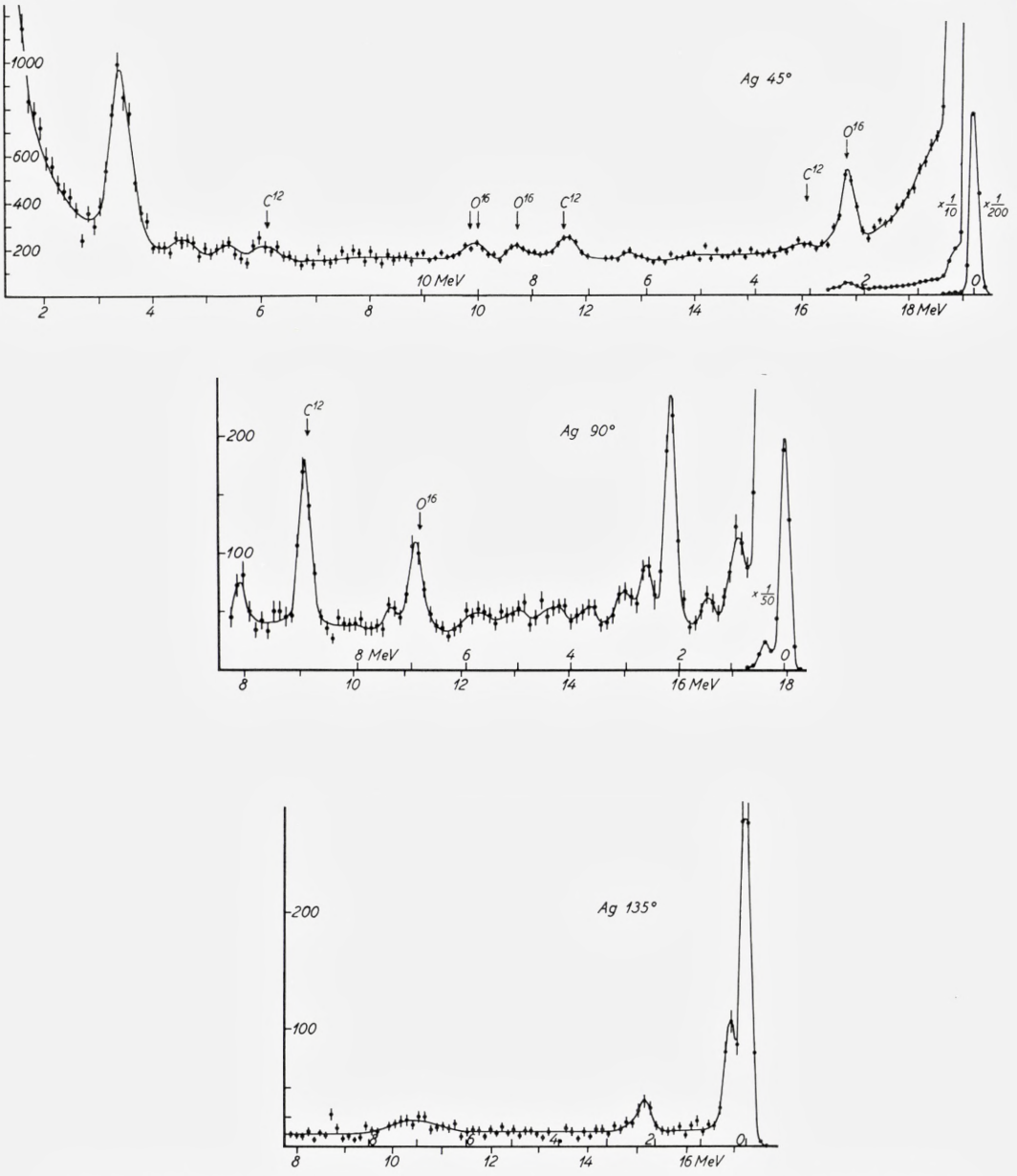

Fig. 10. Spectra of α-particles scattered from a silver foil. Target thickness 0.12 mg/cm² for 45°, 0.48 mg/cm² for 90° and 135°. Integrated doses of primary α's 100, 140, and 101 μ Coulomb for 45°, 90°, and 135°, respectively.

at 45° a bump on the curve, corresponding to about 350 keV. In Table 7, the estimated cross sections are compared with the calculated cross section for Coulomb excitation of the 400 keV-levels*. In view of the large experimental uncertainties the agreement is rather good for the 45°-direction. At 90°, and especially at 135°, the calculations may be expected to give too high values, since they are based upon the classical orbit picture and assuming the α-particle to move in Rutherford orbits. The experimental cross sections seem to vary in accordance with this. However, the results are insufficient to show whether Coulomb excitation is responsible for the peaks or whether other processes are involved.

TABLE 6. Silver

Known levels in				Cohen's peaks	Q-values of peaks		
Ag^{107}		Ag^{109}			45°	90°	135°
0.32	0.42	0.31	0.41	0.39	~ 0.4	~ 0.35	~ 0.3
				0.94		0.85	
				1.50		1.5	
				2.19	(O^{16})	2.18	2.20
						2.6	

All values in the table in MeV.

TABLE 7. Cross section in mb/ster. for the 3–400 keV levels in silver

	45°	90°	135°
Calculated for Coulomb excitation	4.2	3.0	2.5
Experimentally.....	7	1.3	0.1

A level at 2.19 MeV is observed; we find it both at 90° and 135°, whereas in the 45°-direction the O^{16} elastic peak makes observation impossible. In the 90°-curve are furthermore seen peaks at about 0.85, 1.5, and 2.6 MeV and several weaker peaks with Q-values $\geqslant 3$ MeV. The former are probably due to Ag; if they were caused by impurities they should be expected to appear also at 45°. The latter are probably also due to some

* Our thanks are due Mag. BRO-JØRGENSEN for calculating the Coulomb cross sections for Ag and Au.

reactions taking place in the Ag nucleus, as will be made plausible by the following considerations.

In the 45°-curve we see an almost horizontal background with a height about 0.1 % of the height of the elastic peak*. The same background is found when using a target of gold or heavier elements and it may be assumed to be caused by a contamination in the primary α-beam of particles scattered along through the tube or by scattering of the secondary α's in the entrance diaphragm of the ionization chamber. For the heavier elements, the height of the background relative to the elastic peak is the same for all three angles. For silver, however, the "background" amounts to about 0.4—0.5 % in the 90°-curve and 3—4 % in the 135°-curve. Thus, in Ag at 45°, the tail accompanying the high elastic peak can account for the whole counting rate, and any inelastic scattering, except the peak at 3–400 keV, is overshadowed, whereas for the two other angles the counting rate is appreciably higher than would correspond to the tail.

In addition to the main background, the 45°-curve shows the O^{16} and C^{12} peaks known from the mylar curve. To the left of the 9.6 MeV C^{12} peak two other small peaks appear. The left one of these might be assigned to a known level of 10.75 MeV in C^{12}. The big peak $\sim$ 3.5 MeV probably represents recoil protons from a surface layer of water**.

Indium

We have used targets of evaporated In-layers on gold and aluminum. At 90° the gold backed target shows, besides the two elastic peaks, two inelastic peaks, both rather broad. At 45° the two inelastic peaks were not seen, but this may be due to the background. The aluminum backed target was not used for the 45°-direction; at the other two angles it shows four levels (see Fig. 11). The data are summarized in Table 8. The four levels we see were also observed by Cohen. He furthermore sees peaks at 0.63 and 3.07 MeV. In fact, in our curves there are indications of a peak at about 0.5 and another in the neighbourhood of 3 MeV, but the number of events is too small to establish their existence.

* Since the peak widths are so small and the elastic peaks only cover a few channels, the peak height is not a good unit. What we find for Ag at 45° and for the heavier elements at all angles is that the height of the background per channel (using a specific channel width) is 0.065 % of the total number of counts in the elastic peak. This value was used when correcting the 45°-curves for Ni, Cu, and Zn.

** The ratio between the areas of this peak and of the O^{16} peak agrees within the limits of experimental errors with the corresponding ratio for the mylar curve. The amount of H_2O is 1.5 $\mu g/cm^2$.

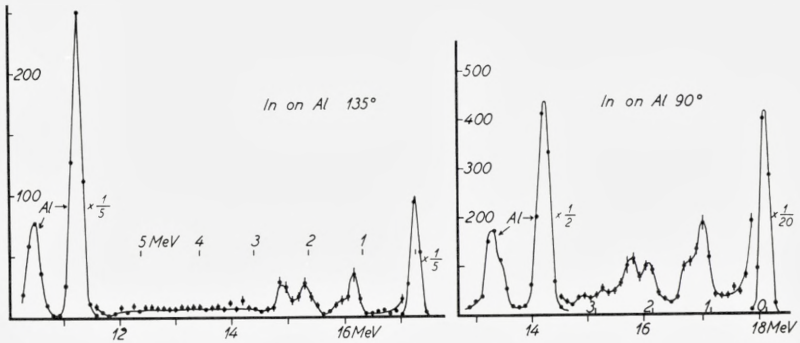

Fig. 11. Spectra of α-particles scattered from a layer of indium evaporated onto a 0.24 mg/cm² aluminum foil. Integrated dose of primary α's 60 and 150 μ Coulomb for 90° and 135°, respectively.

Gold

From the scattering spectra of gold, shown in Fig. 12, only one excited level can be identified. In the 90°-curve a peak is clearly seen at a position corresponding to the known 550 keV-level. A chemical analysis shows, however, the presence of silver in the gold foil, and the silver elastic peak should occur just here. Mag. B. Elbek kindly made a quantitative measurement. He used 4 MeV protons from the Van der Graff and measured the scattered protons by means of a heavy-particle spectrometer and photographic plates. The number of silver atoms in the gold is 15.3 % of the total number of atoms. Since this is not sufficient to account for the observed peak we think we see the 550-keV level. It also appears in the

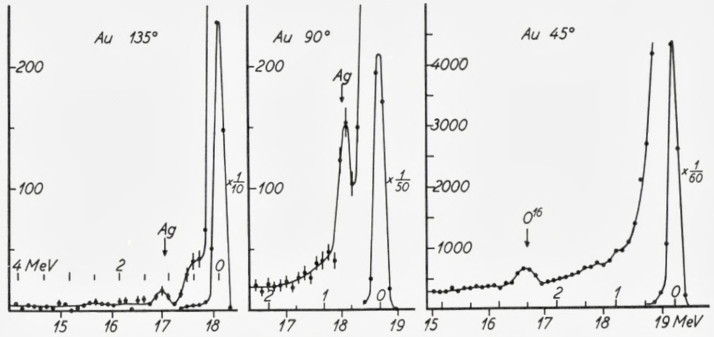

Fig. 12. Spectra of α-particles scattered from a gold foil 0.16 mg/cm². The foil contains 15 % of silver. Integrated doses of primary α's 40, 40, and 100 μ Coulomb for 45°, 90°, and 135°, respectively.

135°-curve clearly separated from the Ag peak; at 45° the elastic peaks from Ag and Au coincide. Here, the 550-keV level is not very pronounced. However, one point lies much higher than the curve and, using the vertical difference between the point and the curve drawn, we obtain the cross section given in Table 9. Here are compared cross sections calculated for Coulomb excitation with the cross sections estimated from the curves. Of course, the "observed" cross sections are very uncertain, since they depend strongly on the way in which the tail of the elastic peak is drawn. Hence, the agreement is satisfactory.

TABLE 8. Indium

Known levels in In^{115} (96 %)	Cohen's peaks	Q-values of peaks	
		90°	135°
0.61	0.63		
0.92			
1.08 1.14	1.14	1.13	1.17
1.29			
	1.48	1.4	1.4
1.98	2.15	2.05	2.07
	2.43	2.43	2.5
	3.07		

TABLE 9. Cross sections in mb/ster. for the 550 keV level in gold

	45°	90°	135°
Calculated for Coulomb excitation	2.2	1.6	1.3
Experimentally.....	2.0	0.9	1.2

Lead and Bismuth

No inelastic scattering was observed in these elements. Curves for Pb on Au and for Bi on Au are very similar to those for pure Au, though the higher elastic peak obscures the 550 keV level in Au.

In Fig. 13 are shown the 45°-curve for Pb on Au, the 90°-curve for Bi on Au, and the 135°-curve for Bi on Al.

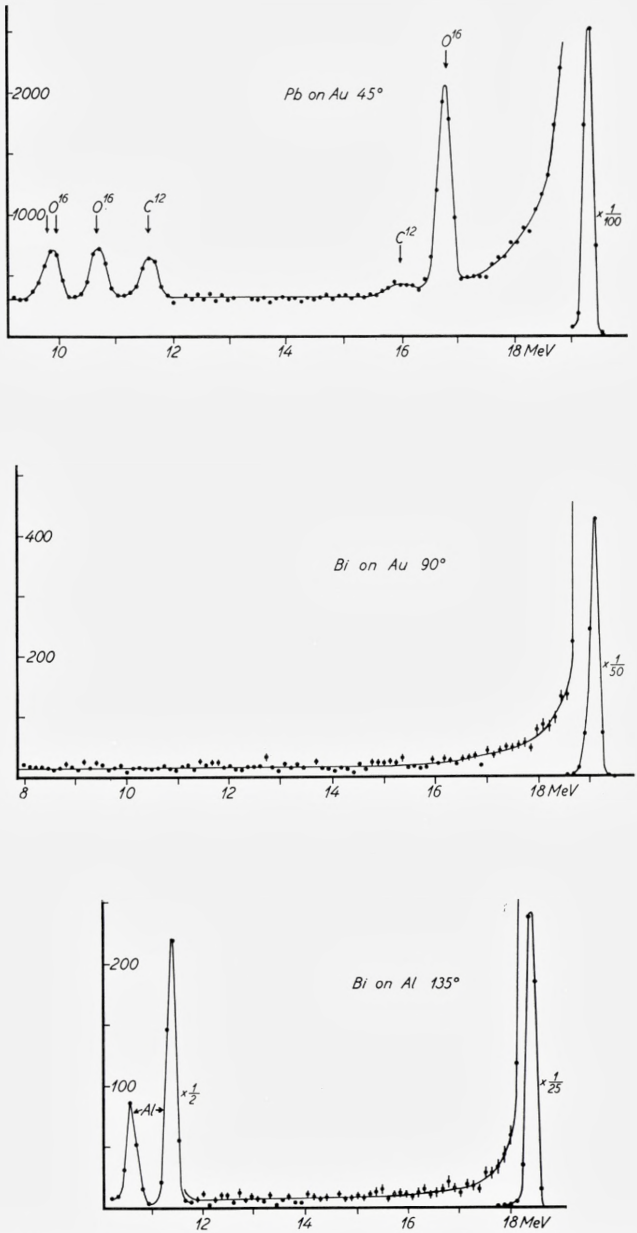

Fig. 13. Spectra of α-particles scattered from layers of lead and bismuth on gold and aluminum. Integrated doses of primary α's 20, 10.4, and 60 μ Coulomb for 45°, 90°, and 135°, respectively.

Width of Peaks

When ΔE is the full width at half maximum height we find for Au $\frac{\Delta E}{E}$ = 1.1 %. From the mylar curve (45°) we get for the elastic O^{16}-peak $\frac{\Delta E}{E}$ = 1.8 %. The mylar target was much thicker than the gold target, but with the transmission geometry used the peak widths should only be very slightly influenced by target thickness and, in fact, from the 45° Pb on Au curve, we find again for the combined Pb and Au peak the half-width 1.1 % and for the O^{16} peak 1.8 %, the latter being corrected for background.

This difference in half-width is due to the geometry. The maximum angular spread caused by the finite size of the ionization chamber window is ± 1°.4, that due to the finite width of the target area ~ ± 0°.5, and that due to the primary beam ~ ± 0°.5. Thus, the total maximum angular spread is ~ ± 2°.4. At 45° scattering angle, this gives a maximum energy spread of 0.54 and 0.06 MeV for O^{16} and Au, respectively. Identifying, for simplicity, half maximum spread and half-width, one calculates from the half-width 0.21 MeV for gold a half-width for O^{16} of $\sqrt{0.21^2+0.24^2} = 0.32$ MeV or 1.8 % of the energy of the elastically scattered α-particles, in agreement with the experimental value.

For some of the targets, for example Cu, the half-width of the elastic peak is somewhat bigger (50 %) than it would be for a thin homogeneous target. We do not know the reason, but suspect target inhomogeneity.

Cross Section for Elastic Scattering

The cross sections obtained for elastic scattering are given in Table 10. They are estimated to be correct within ± 20 %, the main contributions to the uncertainty coming from the beam measurement and from target thickness. No test of foil homogeneity was made.

For gold at 45° we find $\sigma = \sigma_R$, the Rutherford cross section. Within the estimated error the same is valid for 90°, but for 135° $\sigma < \sigma_R$. Looking at elements heavier than aluminum, the well-known variation[6] of σ/σ_R is found. For each element it decreases with increasing scattering angle. It decreases with decreasing atomic number of the scatterer. For the lighter elements the cross section varies in a more irregular manner. For C^{12} at 90° our value agrees fairly well with RASMUSSEN, MILLER, and SAMPSON's value[7]. At 45° our values agree with the values of BLEULER and TENDAM[8] and of

TABLE 10. Cross sections for elastic scattering

	45°			90°			135°		
	σ	σ/σ_R	E_1	σ	σ/σ_R	E_1	σ	σ/σ_R	E_1
Au	3900	1.1	20.0	250	0.85	20.0	70	0.65	19.8
Ag	1200	0.9	20.0	10	0.09	19.8	0.8	0.02	19.8
Zn	170	0.3	19.7	1.2	0.02	19.8	0.32	0.018	20.0
Cu	160	0.3	19.7	1.4	0.03	19.5	0.30	0.018	19.8
Ni	140	0.3	19.6	1.0	0.03	19.9	0.33	0.02	20.0
Al	17	0.22	20.1	0.57	0.07	20.2	0.8	0.22	20.0
O^{16}	45	1.6	19.9	0.3	0.1	20.0	6.4	4.0	19.9
C^{12}	4.6	0.3	19.9	3.9	2.2	20.0	3.2	3.5	19.9

σ is given in millibarns per steradian.

E_1 is the energy in MeV of the α-particles having traversed half the thickness of the scattering foil.

The thickness of the Zn-layer was chosen to 1.1 mg/cm² in order to obtain the above figures.

O. GAILAR[9] for Ag, Cu, and Al. For Ag we find somewhat lower values for σ/σ_R at 90° and 135° than Gailar, but since his α-energy (18.7 MeV) is lower than ours this should be expected. For Cu the agreement is good; for Al a comparison is not justified, since the cross section may vary considerably with energy.

4. Discussion

The elements we have studied may be divided into four groups:

I. The light elements C, O, Mg, and Al.
II. The medium light elements Ni, Cu, and Zn.
III. The medium heavy elements Ag and In.
IV. The heavy elements Au, Pb, and Bi.

Group I

The spectra of α-particles scattered from the elements of group I are composed of single peaks. For carbon and oxygen, these peaks correspond to known levels which are widely spread. For magnesium, peaks due to Mg^{24} are dominant, even though the rarer isotopes Mg^{25} and Mg^{26} have more low-lying excited states. For aluminum, the spectra are more complex,

showing many closely packed peaks. Common to all spectra are single peaks seen up to excitation energies of about 10 MeV. We cannot see peaks for higher excitation energies, because we then get into the intense continuous spectrum due to protons.

Two possible processes through which one can imagine that scattering occurs have already been mentioned. The first involves compound nucleus formation followed by the evaporation of a particle. The second, the so-called direct interaction process, involves a collision between the incoming particle and one (or at most a few) nucleons. The first process requires a much longer average time per event than does the second one.

One way of determining which of these proposed mechanisms is effective in a particular case is to study the angular distribution of α-particles corresponding to a definite level in the residual nucleus. If the scattering occurs entirely through compound nucleus formation, a distribution symmetrical about 90° is expected, whereas if the direct interaction process is dominant, the angular distribution should be peaked more or less in the forward direction. For Mg^{24} and other light nuclei, WATTERS[10] has found results strongly supporting the direct interaction picture. The angular distributions show maxima and minima which may be largely accounted for by theoretical considerations[1].

When looking only at a few definite angles, as we have done, one may expect to find intensities of the various inelastic peaks varying in an irregular manner, since the intensity will depend on whether the particular angle is close to a maximum or to a minimum. Our results for C, O, and Mg are in accordance with this expectation.

For aluminum, however, we find a somewhat more regular variation. The ratio R_1 between peak heights at 45° and 90° (Table 2) is high (35) for the elastic peak. For the first excited state it is somewhat lower (5.8), and it decreases with increasing excitation energy until, for the fifth level, it reaches a value between one and two, and then remains fairly constant with further increasing excitation energy. For the low-lying levels, the lack of symmetry around 90° and the strong forward peaking may be taken as an indication of a direct interaction.

For the higher excitation energies, the fact that single peaks are observed may give rise to some speculation. Assuming the level spacing here to be quite small, which may be justified in view of the high angular momenta involved, this would seem to point to some mechanism different from compound nucleus formation. Professor AAGE BOHR has suggested that the α-particle stays long enough in the nucleus to transfer energy to a small num-

ber of nucleons, but not so long that the energy is distributed over a larger fraction of the nucleons. Another viewpoint would be to assume a somewhat higher level spacing comparable with our resolution. In this case, compound nucleus scattering would just give curves like ours with single peaks showing up on top of a continuous background. Anyhow, whether the single peaks are due to the one or the other process, we do see an increasing continuous background for excitation energies above some 4 MeV, and this background is interpreted as due to α-particles boiled off from the compound nucleus.

Group II

If the compound nucleus interpretation is correct, one might expect to find a similar behaviour for heavier nuclei, but with higher cross sections for the compound nucleus contribution because of the higher level densities. This agrees well with our results for Ni, Cu, and Zn. For these elements we see, in addition to the single peaks, a broad continuous distribution between 5 and 14 MeV, which we ascribe to compound scattering. The shape of this evaporation spectrum has been compared with the statistical theory, which gives the formula[11]

$$N(E)\,dE = \text{const.}\ \varrho(E^*)\cdot E\sigma_c(E)\,dE, \qquad \text{(I)}$$

where E is the total kinetic energy of the evaporated α-particle and the residual nucleus in the center of mass system, N is the intensity of α-particles of this particular energy, $\sigma_c(E)$ is the cross section for formation of the compound nucleus when bombarding with α-particles of this energy, and $\varrho(E^*)$ is the level density of the residual nucleus at an excitation energy $E^* = E_0 - E$. E_0 is the energy in the entrance channel.

Rearranging the formula, we get

$$\log \varrho(E^*) = \log N(E) - \log \frac{\sigma_c(E)}{\pi \lambda\!\!\!^{-2}} + C. \qquad \text{(II)}$$

The second term on the right side was calculated by means of table IV in the paper of SHAPIRO[12]. The interaction radii 7.66, 7.81, and 7.86 Fermis for Ni, Cu, and Zn, respectively, determined by KERLEE, BLAIR, and FARWELL[6], were used to obtain the values of the Coulomb barrier. Plotting $\log(N(E)) - \log \frac{\sigma_c(E)}{\pi \lambda\!\!\!^{-2}}$ against E^*, we get straight lines as shown in Fig. 14. We may then write

$$\varrho\,(E^*) = \text{const.} \times \exp. \frac{E^*}{T}, \qquad \text{(III)}$$

where T is a constant. Defining in the usual way the nuclear temperature as $\left(\frac{d \log \varrho}{dE^*}\right)^{-1}$ we thus find this temperature T to be constant. The values found for T are given in Table 11.

TABLE 11. Nuclear temperature T in MeV as derived from the α-spectra

	135°	90°	45°
Ni	1.15	1.06	(1.16)
Cu	1.16	1.16	(1.25)
Zn	1.04	1.03	(1.15)

When calculating the temperature the experimental points were not directly used, but points were chosen on the dashed lines shown in Figs. 7—9. In this way, a separation between the α-particles scattered in direct interactions and *via* a compound nucleus was attempted, and also the peaks due to impurities were omitted. From the curves it is evident that the 45°-results are much more uncertain than the 90°–and 135°-results.

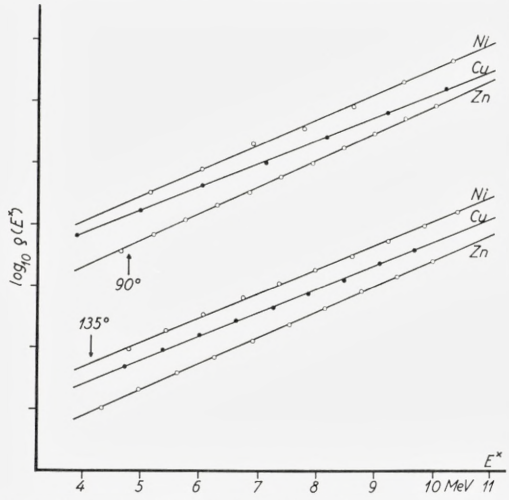

Fig. 14. Level density functions as obtained from the spectra of scattered α's from Ni, Cu, and Zn. The ordinate is $\log N(E) - \log \frac{\sigma_c\,(E)}{\pi \lambda^2} = C + \log \varrho\,(E^*)$. The lines drawn correspond to $\varrho\,(E^*) \sim \exp \frac{E^*}{T}$ with the T-values given in Table 11.

The figures for 45° are given here mainly to show that compound scattering is also observed at this angle. An error in the earlier mentioned background associated with the high elastic peaks—the horizontal dashed lines—will influence the T-values. Another very likely reason for the higher temperatures found from the 45°-curves is that direct processes may play a larger role than would correspond to the dashed lines.

The error in R given by Kerlee, Blair and Farwell is $\Delta R = \pm 0.13$ Fermis, which gives $\Delta T = \pm 0.02$ MeV. For the 90°–and 135°–results, we estimate the total erorr to be $\Delta T \sim \pm 0.04$ MeV.

It is interesting to see that the temperature is higher for copper than for nickel and zinc. Since copper consists of two odd-even isotopes, whereas the predominant isotopes in nickel and zinc are even-even, such a difference would not be unexpected. However, the difference is not much outside the experimental uncertainty and further data are needed to ensure the significance of it.

It should be stressed that the estimates of temperature were obtained by treating our experimental results in the particular manner described, i. e., on the basis of a model of the reaction in which a sharply defined interaction radius $R = 7.66$ Fermis was assummed. Smaller R-values in a reasonable range also give approximately straight lines in the $\log \varrho$ *vs* E^* plots, but with slopes corresponding to lower temperatures, the T-values being roughly propertional to the R-values used. Significantly larger values of R, however, give curved lines in such plots.

For further comparison with the statistical theory, the cross section for compound nucleus scattering was calculated, using the expression

$$\sigma_{\alpha,\alpha'} = \sigma_{c,\alpha}(E_0) \times \frac{M_\alpha \int_0^{E_0} E\sigma_{c,\alpha}(E)\varrho_1(E^*)\,dE}{M_\alpha \int_0^{E_0} E\sigma_{c,\alpha}(E)\varrho_1(E^*)\,dE + 2M_p \int_0^{E_1} E\sigma_{c,p}(E)\varrho_2(E^*)\,dE + 2M_n \int_0^{E_2} E\sigma_{c,n}(E)\varrho_3(E^*)\,dE}. \quad \text{(IV)}$$

Here, $\sigma_{\alpha,\alpha'}$ is the cross section for compound nucleus scattering; $\sigma_{c,\alpha}(E)$, $\sigma_{c,p}(E)$, $\sigma_{c,n}(E)$ are the cross sections for formation of the compound nucleus when bombarding the respective residual nuclei with α-particles, protons, and neutrons, respectively, of energy E; M_α, M_p and M_n are the reduced masses of the α-particle, the proton, and the neutron, respectively; E_0 is the entrance channel energy (C. M. system); E_1 and E_2 are the maximum channel energies for outgoing protons and neutrons, respectively;

$\varrho_1(E^*)$, $\varrho_2(E^*)$, $\varrho_3(E^*)$ are the level density functions for the residual nuclei corresponding to α-, proton-, and neutron-emission, respectively, and the factor 2 for protons and neutrons takes into account the statistical weight due to spin.

Consider, for example, the scattering from Cu^{63}

$$Cu^{63} + \alpha \rightarrow (Ga^{67})^* \rightarrow \begin{cases} Cu^{63} + \alpha \\ Zn^{66} + p \\ Ga^{66} + n \end{cases}$$

We neglect γ-transitions. Deuteron emission is calculated to be negligibly small.

Now ϱ_1, ϱ_2, and ϱ_3 are the level density functions of Cu^{63}, Zn^{66}, and Ga^{66}. These are not known, but the temperatures may be expected to be nearly the same for neighbouring nuclei, as is also borne out by Table 11, and hence a good approximation should be to put

$$\varrho = K \cdot exp\left(\frac{E^*}{1.08}\right) \qquad (V)$$

for all these nuclei. The proportionality factor K is, however, different for odd and even nuclei due to pairing correlations between the nucleons. This has roughly the effect of increasing the excitation energy by δ for odd-even and by $2\,\delta$ for odd-odd nuclei, where δ is half the pairing energy[14, 15, 18], or to increase ϱ by $exp\left(\frac{\delta}{T}\right)$ for odd-even and by $exp\left(\frac{2\delta}{T}\right)$ for odd-odd nuclei.

Since $\delta \approx T$, we therefore put for the nuclei here considered K = k, 3 k, and 9 k for even-even, odd-even, and odd-odd nuclei, respectively.

The E_1- and E_2-values were determined from Wapstra's tables[16]. In evaluating the integrals, Shapiro's tables were used for $\sigma_{c,\alpha}$ and $\sigma_{c,p}$. For the nuclear radii were used $R = 1.414 \cdot A^{1/3} + 2.19$ Fermis, where the last term was omitted for protons and neutrons. For neutrons, the cross sections given in Blatt and Weisskopf[17] were used.

The calculations give for Cu^{63}

$$\sigma_{\alpha,\alpha'} = 0.954 \frac{14}{14 + 24 + 62} = 0.128 \text{ barns.}$$

The results of calculations for some target nuclei are given in Table 12, and in Table 13 the experimental cross sections are compared with the calculated values. The experimental cross sections are about equal for the three directions, as should be expected for compound nucleus scattering.

The slightly high values for 45° probably again show that the correction for direct processes, indicated by the dotted line, is insufficient. As the best value for the average cross section we take a weighted mean using arbitrary weight factors 2, 2, and 1 for 135°, 90°, and 45°, respectively.

TABLE 12

Target nucleus	Percentage of		
	α's	p's	n's
Ni^{60}	14	37	49
Cu^{63}	14	24	62
Cu^{65}	4	4	92
Zn^{66}	12	15	73

TABLE 13. σ in millibarn per steradian

Target	Experimental			Weighted mean	Calculated		
	135°*)	90°*)	45°*)		for		$\sigma exp/\sigma calc.$
Nickel	8.5	5.5	8.6	7.3	Ni^{60}	10.0	0.73
Copper	5.8	4.0	7.6	5.4	nat. Cu.	8.0	0.68
Zink	6.6	3.9	9.1	6.0	Zn^{66}	9.6	0.63

The angles are in the laboratory system. The cross sections have been corrected for C. M. motion.

The agreement between the absolute values of the calculated and the measured cross sections is better than to a factor of two, which is satisfactory. In view of the uncertainties in the parameters, one could hardly expect closer agreement, and the results show that we may be confident in regarding the α-particles as being evaporated from the compound nucleus. The ratio between the calculated cross sections for the three elements reproduce the experimental values to a much higher accuracy, which is further corroboration that, so far as the continuum is concerned, the scattering process proceeds mainly through compound nucleus formation.

It may be noted that, if the different odd-even factors in the expression (V) for ϱ had not been applied, the agreement between calculated and experimental absolute cross sections would have been poorer, and especially that $\sigma exp/\sigma calc.$ would have been twice as high for the copper as for the two other targets.

It may be argued that, although the previous considerations strongly support the statistical theory, the level density function $\varrho = k \exp\left(\frac{E^*}{T}\right)$, where T is a constant, is not what should be expected. The free-particle Fermi gas theory predicts $\varrho = k \exp\left((aE^*)^{\frac{1}{2}}\right)$. It would therefore seem to be interesting to plot $\log N(E) - \log \frac{\sigma_c(E)}{\pi \lambda^2}$ as a function of $\sqrt{E^*}$. This is done in Fig. 15.

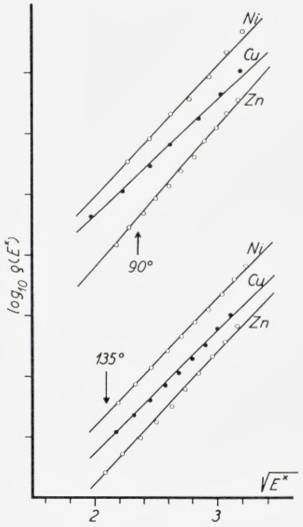

Fig. 15. The level density plotted as a function of $\sqrt{E^*}$.

The fit to straight lines is definitely worse in this plot than in Fig. 14; actually, in all cases, the points indicate a curved line. In passing, it may be mentioned that the use of smaller R-values would give stronger curvatures. In Fig. 15, the straight lines drawn for Ni, Cu, and Zn at 90° correspond to $a = 6.1$, 4.8, and 7.2, and at 135° to $a = 5.7$, 5.3 and 6.2, respectively, a being in MeV^{-1}. It is thought that the correlations between the motions of the nucleons are causing considerable deviations from the free-particle Fermi gas picture at low excitation energies, associated particularly with the existence of pairing effects. When these are taken into account, the nuclear temperature is expected to vary only slowly with energy in an intermediate energy range* **[15, 18], and it is therefore not surprising that we find a nearly constant temperature in the range 4–10 MeV.

* V. F. Weisskopf: private communication.
** V. Strutinski: private communication.

In Fig. 16, we have attempted a comparison with some other experimental determinations of the level density of nuclei in the copper region. Here is plotted the ratio $\varrho(E^*):\varrho(1)$ between level densities at excitation energies E^* and 1 MeV. Curve a is the level density found in this experiment. Curve b is that found in (α, p) experiments by EISBERG, IGO, and WEGNER[19]. Curve c is the one found by GUGELOT[20] by (p, p') scattering experiments. For the latter work it is now generally agreed, we think, that direct processes overshadow the compound scattering at small excitation energies. At high energies, curves a and c tend to become parallel; in the

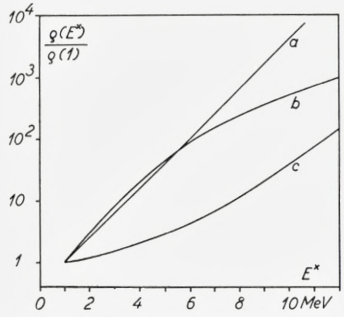

Fig. 16. Comparison with some other experimental level densities for elements in the copper region. Level density determined:

a) from (α, α') reactions is this work;
b) from (α, p) reactions (ref. 19) on Cu;
c) from (p, p') reactions (ref. 20) on Cu.

energy region 10–13 MeV the temperature as given by Gugelot is 1.2 MeV, in good agreement with our value of 1.1 MeV. For low energies, curves a and b agree fairly well, but for higher energies, a difference is observed which is not understood.

More recently, MARCH and MORTON[21] have studied (n, p) reactions in Fe^{54} and Fe^{56}, using 13.5 MeV neutrons; they found a shape of the energy distributions of emitted protons consistent with the statistical theory and corresponding to a temperature of about 1.2 MeV. In similar experiments, ALLAN[22] found for $Cu(n, p)$ Ni reactions a temperature of 1.0 MeV. ZUCKER[13], studying the reactions

$$_{13}Al^{27} + {}_{7}N^{14} \rightarrow {}_{20}Ca^{41} \rightarrow \begin{cases} {}_{19}K^{40} + p \\ {}_{18}A^{37} + \alpha, \end{cases}$$

found for both residual nuclei densities $\varrho \sim exp\sqrt{aE^*}$. His results cover a large energy region. Replotting his values for $\dfrac{N(E)}{E\sigma_c(E)}$ as a function of E^*,

we find in a limited interval—for α-particles between 5 and 12 MeV—rather good agreement with $\varrho \sim exp\ E^*/T$ with a temperature of about 1.5—1.6 MeV. Since the nuclei involved here are much lighter than in our case the higher temperature is not surprising. The interesting feature is that, in the energy interval covered in our experiments, also Zucker's results agree with a level density function $\varrho \sim exp\ E^*/T$ with a constant temperature, whereas his results show that, for higher excitation energies, the temperature varies with E^*.

Group III

For Ag and In, a calculation shows that the number of α-particles to be expected from compound nucleus scattering is orders of magnitude smaller due to the higher Coulomb barrier. In accordance with this evidence we do not see any evaporation distribution, but only a few single peaks probably due to direct interactions.

Group IV

For Au, Pb, and Bi, the Coulomb barrier is so high that the probability that an α-particle will penetrate it twice—in and out—is very small. Accordingly, we have observed no nuclear processes except Coulomb interactions, which we have seen only in Au.

These experiments were carried out at the Institute for Theoretical Physics, University of Copenhagen, and the authors wish to express their gratitude to the Director of the Institute, Professor Niels Bohr, for his interest in the work. For many valuable discussions our thanks are due Dr. Torleif Ericson, Dr. Ben Mottelson, Professor Aage Bohr, and many others. We should also like to thank Mr. Philip Dam for his help in operating the cyclotron and Miss Lise Bryde for doing most of the numerical calculations. One of us (HWF) also wishes to thank the Guggenheim Foundation and the United States Educational Foundation in Denmark for support during his year's stay at the Institute.

References

(1) S. Butler: Phys. Rev. **106**, 272, 1957.
(2) B. L. Cohen: Phys. Rev. **105**, 1549, 1957.
(3) W. G. Cross: Rev. Sc. Instr. **22**, 717, 1951.
(4) M. Mazari, W. W. Buechner, and R. P. de Figueiredo: Phys. Rev. **108**, 373, 1957.
(5) B. L. Cohen, and A. G. Rubin: Phys. Rev. **111**, 1568, 1958.
(6) D. D. Kerlee, J. S. Blair, and G. W. Farwell: Phys. Rev. **107**, 1343, 1957.
(7) V. K. Rasmussen, D. W. Miller, and M. B. Sampson: Phys. Rev. **100**, 181, 1955.
(8) E. Bleuler, and D. J. Teendam: Phys. Rev. **99**, 1605, 1955.
(9) O. Gailar: USAEC Progress Report No. 6, Purdue, Lafayette, Indiana. COO–173.
(10) H. J. Watters: Phys. Rev. **103**, 1763, 1956.
(11) J. M. Blatt, and V. F. Weisskopf: Theoretical Nuclear Physics, John Wiley and Sons, New York 1952.
(12) M. Shapiro: Phys. Rev. **90**, 171, 1953.
(13) A. Zucker: Nucl. Phys. **6**, 420, 1958.
(14) T. D. Newton: Can. J. Phys. **34**, 804, 1956.
(15) T. Ericson: Nucl. Phys. **6**, 62, 1958.
(16) A. H. Wapstra: Physica XXI, 385, 1955.
(17) See ref. 11, Fig. 4.2, p. 348.
(18) T. Ericson: Nucl. Phys. **8**, 265, 1958.
(19) R. M. Eisberg, G. Igo, and H. E. Wegner: Phys. Rev. **100**, 1309, 1955.
(20) P. C. Gugelot: Phys. Rev. **93**, 425, 1953.
(21) P. March, and W. T. Morton: Phil. Mag. **3**, 143, 1958.
(22) D. L. Allan: Nucl. Phys. **6**, 464, 1958.

Indleveret til selskabet den 2. juli 1958.
Færdig fra trykkeriet den 16. marts 1959.